THE TRANSIT LIGHT CURVE PROJECT. VII. THE NOT-SO-BLOATED EXOPLANET HAT-P-1b

JOSHUA N. WINN,[1] MATTHEW J. HOLMAN,[2] GASPAR Á. BAKOS,[2,3] ANDRÁS PÁL,[4]
JOHN ASHER JOHNSON,[5] PETER K. G. WILLIAMS,[5] AVI SHPORER,[6] TSEVI MAZEH,[6]
JOSÉ FERNANDEZ,[2,7] DAVID W. LATHAM,[2] AND MICHAEL GILLON[8]

ABSTRACT

We present photometry of the G0 star HAT-P-1 during six transits of its close-in giant planet, and we refine the estimates of the system parameters. Relative to Jupiter's properties, HAT-P-1b is 1.20 ± 0.05 times larger, and its surface gravity is 2.7 ± 0.2 times weaker. Although it remains the case that HAT-P-1b is among the least dense of the known sample of transiting exoplanets, its properties are in accord with previously published models of strongly irradiated, coreless, solar-composition giant planets. The times of the transits have a typical accuracy of 1 minute and do not depart significantly from a constant period.

Key words: planetary systems — stars: individual (HAT-P-1, ADS 16402B)

Online material: machine-readable table

1. INTRODUCTION

More than 12 years have passed since the surprising discovery of "hot Jupiters," giant planets around Sun-like stars with orbital periods smaller than ~10 days (Mayor & Queloz 1995; Butler et al. 1997). These objects, of which about 50 are known (see, e.g., Butler et al. 2006), probably formed at larger orbital distances and migrated inward through processes that are not yet fully understood. Hot Jupiters are also interesting because they are more likely to transit their parent stars than more distant planets. Transits are highly prized because they permit the determination of the planetary radius and mass (Henry et al. 2000; Charbonneau et al. 2000), the infrared planetary spectrum (Richardson et al. 2007; Grillmair et al. 2007) and longitudinal brightness profile (Knutson et al. 2007b), the stellar obliquity (Winn et al. 2007a), and much more. This helps to explain why so many groups around the world are conducting wide-field photometric surveys for planetary transits. Over a dozen cases of transiting exoplanets have been identified in this manner, with the rest having been found as a by-product of Doppler planet surveys (see Charbonneau et al. 2007 for a recent review).

Recently, the Hungarian-made Automated Telescope Network (HATNet) announced the discovery of HAT-P-1b, a giant planet that orbits one member of a G0/G0 stellar binary (Bakos et al. 2007). This planet is notable for being among the largest and least dense of all the planets for which such measurements have been made—both inside and outside the solar system—and is therefore an interesting test case for models of planetary atmospheres and interiors.

However, while the data presented by Bakos et al. (2007) were certainly good enough to clinch the case for planethood and to provide useful estimates of the system parameters, it is possible and desirable to improve the accuracy of those parameters with repeated, high-precision, ground-based transit photometry. This is one goal of our Transit Light Curve (TLC) Project, which has been described at greater length elsewhere (see, e.g., Holman et al. 2006; Winn et al. 2007b).

This paper presents our results for the HAT-P-1 system. The next section describes the observations. In § 3 we describe the parametric model that was fitted to the data, and in § 4 we present the results for the planetary, stellar, and orbital parameters, as well as the transit times. At the end of this paper we discuss the significance of the refined radius measurement.

2. OBSERVATIONS AND DATA REDUCTION

Our observations took place in late 2006, using telescopes at three different observatories. We observed six distinct transits and produced seven independent light curves.

We observed the transits of UT 2006 September 18, September 27, and October 6 with the 1.2 m telescope at the Fred L. Whipple Observatory (FLWO) on Mount Hopkins, Arizona. We used the 4096^2 KeplerCam CCD, which has a $23.1' \times 23.1'$ field of view. We employed 2×2 binning, giving a scale of $0.68''$ per binned pixel, a readout and setup time of 11 s, and a typical readout noise of $7\ e^-$ per binned pixel. We used a Sloan z filter in order to minimize the effect of atmospheric extinction on the relative photometry and the effects of stellar limb darkening on the transit light curve. We kept the image registration as constant as possible. We also obtained dome-flat and bias exposures at the beginning and the end of each night. On September 18 the sky conditions were photometric and the seeing varied from $1.7''$ to $2.1''$. We used an exposure time of 15 s. The night of September 27 began with patchy clouds and large transparency variations, but the rest of the night was clear. The seeing varied between $1.7''$ and $2.4''$, and we again used an exposure time of 15 s. Most of October 6 was lost to clouds, although we did manage to observe the egress in $1.8''$ seeing, using an exposure time of 10 s.

[1] Department of Physics and Kavli Institute for Astrophysics and Space Research, Massachusetts Institute of Technology, Cambridge, MA 02139, USA.

[2] Harvard-Smithsonian Center for Astrophysics, 60 Garden Street, Cambridge, MA 02138, USA.

[3] Hubble Fellow.

[4] Department of Astronomy, Eötvös Loránd University, Pf. 32, H-1518 Budapest, Hungary.

[5] Department of Astronomy, University of California, Mail Code 3411, Berkeley, CA 94720, USA.

[6] Wise Observatory, Raymond and Beverly Sackler Faculty of Exact Sciences, Tel Aviv University, Tel Aviv 69978, Israel.

[7] Department of Astronomy, Pontificia Universidad Católica, Casilla 306, Santiago 22, Chile.

[8] Observatoire de l'Université de Genève, 1290 Sauverny, Switzerland; and Institut d'Astrophysique et de Géophysique, Université de Liège, 4000 Liège, Belgium.

We observed the transits of UT 2006 September 1, September 10, and September 18 using the Nickel 1 m telescope at Lick Observatory on Mount Hamilton, California. The only night when a complete transit could be observed was September 18. We used the Dewar No. 2 direct imaging detector, which is a 2048^2 Lawrence Labs CCD with a $6.1' \times 6.1'$ field of view. For our observations we used 2×2 binning ($0.36''$ per binned pixel) and read out only a 1450×500 pixel subregion of the chip to decrease the readout time. Setup and readout time took about 10 s per exposure, with a typical read noise of 11.8 e^- per binned pixel. We observed through a "Gunn Z" filter (Pinfield et al. 1997). To draw out the exposure time and to spread the light from stars over more pixels, we defocused the telescope until the stellar images had a full width at half-maximum (FWHM) of about 6 pixels. The exposure time ranged from 10 to 40 s, depending on seeing and transparency. All nights were fairly clear, with $1.0''-1.5''$ seeing. On September 18, near the transit midpoint, the star passed within a few degrees of the zenith, and autoguiding failed. The data from that time period were excised.

We observed the transits of UT 2006 September 14, November 20, and November 29 using the 1 m telescope at Wise Observatory in Israel. We used a Tektronix 1024^2 back-illuminated CCD detector, giving a pixel scale of $0.7''$ and a field of view of $11.9' \times 11.9'$. We observed through a Johnson I filter, the reddest optical band available on the camera. On September 14 and November 20, weather conditions were poor, with patchy clouds. Because the data from those nights were of much lower quality than the other data presented in this paper, in what follows we describe only the data from 2006 November 29. The night was not photometric, and the measured stellar fluxes varied by about 20% over the course of the night. The exposure time was 15 s, and the FWHM of the stellar images was about $1.8''$ (2.5 pixels).

We used standard IRAF[9] procedures for overscan correction, trimming, bias subtraction, and flat-field division. We performed aperture photometry of HAT-P-1 and four to eight nearby stars, depending on the telescope. The sum of the fluxes of the comparison stars was taken to be the comparison signal. The light curve of HAT-P-1 was divided by the comparison signal and then divided by a constant to give a unit mean flux outside of transit.

We then assessed residual systematic effects by examining the correlation between the out-of-transit flux and some external variables: time, air mass, the shape parameters of the stellar images, and the pixel position of HAT-P-1. For the FLWO data, the flux variations were most strongly correlated with air mass; for the Lick data, the strongest correlations were with the pixel coordinates, especially the row number; and for the Wise data, there were correlations with both air mass and the FWHM of the stellar images (which were themselves strongly correlated). We solved for the zero point and slope of the strongest correlation as part of the fitting process described in the next section.

Figures 1 and 2 show the final light curves. The bottom panel of Figure 2 is a phase-averaged composite of the three best light curves. Table 1 provides the final photometry, after correction of the residual systematic effects.

3. DETERMINATION OF SYSTEM PARAMETERS

To estimate the planetary, stellar, and orbital parameters and the times of transit, we fitted a parameterized model to the photo-
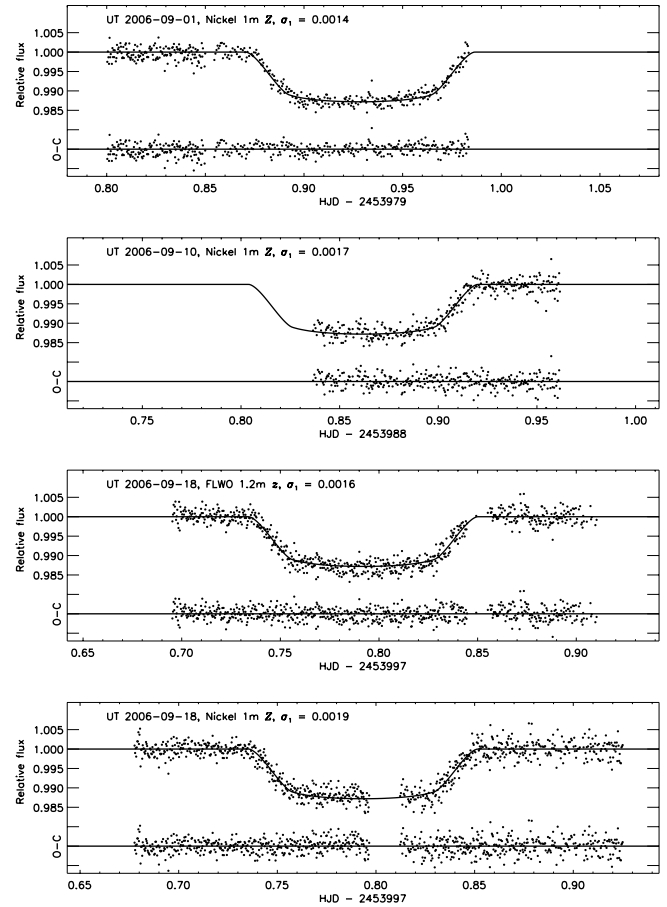

Fig. 1.—Relative photometry of HAT-P-1. The residuals ($O - C$) are plotted beneath the data.

metric data. The model and the fitting method are similar to those described in previous TLC papers (see, e.g., Holman et al. 2006; Winn et al. 2007b). The model is based on a circular orbit[10] of a star (with mass M_* and radius R_*) and a planet (M_p, R_p) about their center of mass, inclined by an angle i relative to the sky plane. Because one of our goals was to measure the individual transit times, we allowed each transit to have an independent value of T_c, the transit midpoint, rather than forcing them to be separated by regular intervals.

The most natural parameters one would like to know are R_* and R_p, but these parameters cannot be determined independently from the data. The relevant parameters that can be determined are R_p/R_* and R_*/a, where a is the orbital semimajor axis. The only property intrinsic to the star that follows directly from the photometric data is the mean stellar density (see, e.g., Seager & Mallén-Ornelas 2003):

$$\rho_* \equiv \frac{M_*}{4/3\pi R_*^3} = \frac{3\pi}{GP^2}\left(\frac{R_*}{a}\right)^{-3}. \qquad (1)$$

In order to determine R_* and R_p independently, one must have an external estimate of R_*, M_*, or some combination of R_* and

[10] This is our default assumption in the absence of clear evidence for an eccentric orbit. Although the orbital fit of Bakos et al. (2007) yielded the formal result $e = 0.09 \pm 0.02$, we regard this as only suggestive. The orbital eccentricity is subject to a positive bias in such fits, because e is positive definite, and experience has shown that indications of a small nonzero eccentricity usually disappear after more velocity data are obtained.
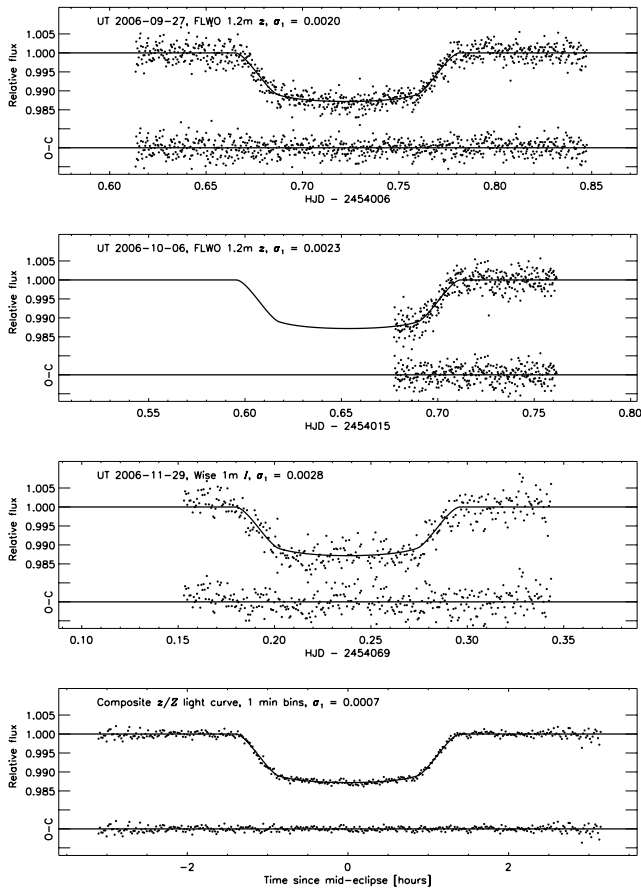
Fig. 2.—Relative photometry of HAT-P-1. The residuals $(O - C)$ are plotted beneath the data. The bottom panel is a composite light curve created from all of the z- and Z-band data by subtracting the best-fitting value of T_c from the time stamps of each light curve and then averaging into 1 minute bins.

TABLE 1

Photometry of HAT-P-1

Telescope	Filter	Heliocentric Julian Date	Relative Flux
FLWO..........	z	2,453,997.69528	0.9988
FLWO..........	z	2,453,997.69560	1.0006
FLWO..........	z	2,453,997.69591	1.0031
FLWO..........	z	2,453,997.69621	1.0009
Lick	Z	2,453,997.91750	1.0013
Lick	Z	2,453,997.91781	0.9965
Lick	Z	2,453,997.91811	1.0016
Wise	I	2,454,069.33838	1.0014
Wise	I	2,454,069.33894	0.9970
Wise	I	2,454,069.33950	1.0000

Notes.—The time stamps represent the Heliocentric Julian Date at the time of midexposure. Table 1 is published in its entirety in the electronic edition of the *Astronomical Journal*. A portion is shown here for guidance regarding its form and content. The data are also available from the authors on request.

intensity over the unobscured portion of the stellar disk. We assumed the limb-darkening law to be quadratic,

$$\frac{I_\mu}{I_1} = 1 - a(1 - \mu) - b(1 - \mu)^2, \qquad (2)$$

where I is the intensity and μ is the cosine of the angle between the line of sight and the normal to the stellar surface. We did not use the "small-planet" approximation. We fixed the limb-darkening coefficients at the values calculated and tabulated by Claret (2004) for observations of a star with the observed spectral properties.[11] We also investigated the effects of changing the limb-darkening law and fitting for the limb-darkening parameters, as discussed below. In addition, as mentioned in the previous section, we fitted for the zero point and slope of the correlation between the measured flux and the external variable that showed the strongest correlation. For the FLWO data this variable was air mass, for Lick it was the column number, and for the Wise data it was the FWHM of the stellar images.

The fitting statistic was

$$\chi^2 = \sum_{j=1}^{N_f} \left[\frac{f_j(\text{obs}) - f_j(\text{calc})}{\sigma_j} \right]^2, \qquad (3)$$

where $f_j(\text{obs})$ is the flux observed at time j, σ_j controls the weights of the data points, and $f_j(\text{calc})$ is the calculated flux. As noted in the previous section, the calculated flux was the idealized flux of a transit light curve after subtracting a linear function of a specified external variable.

For the data weights σ_j, many investigators use the calculated Poisson noise, or the observed standard deviation of the out-of-transit data. Experience has shown that these procedures usually result in underestimated uncertainties in the model parameters, because they neglect time-correlated errors ("red noise"; see, e.g., Gillon et al. 2006), which are almost always significant for ground-based data. In order to derive realistic uncertainties on the parameters, it is important for σ_j to take red noise into account, at least approximately.

M_* besides ρ_*. This external estimate may come from supplementary observations, such as the stellar angular diameter and parallax (see, e.g., Baines et al. 2007), or from the interpretation of the stellar spectrum with theoretical model atmospheres and evolutionary tracks. The comparison with theory can be facilitated by the estimate of ρ_* that comes from the photometry, because the photometric estimate is often more precise than the traditional spectroscopic gravity indicator, $\log g$ (see, e.g., Pont et al. 2007; Sozzetti et al. 2007; Holman et al. 2007).

Our approach is to fix M_* at a fiducial value and then determine R_* and R_p from the light curve. The scaling relations $R_* \propto M_*^{1/3}$ and $R_p \propto M_*^{1/3}$ may then be used to estimate the resulting systematic error due to the uncertainty in the stellar mass. This also makes it easy to update the determinations of R_* and R_p as our understanding of the host star is revised through further observations and analyses. In this case, we assume $M_* = 1.12\,M_\odot$, based on the analysis by Bakos et al. (2007) in which the spectroscopic properties of both members of the stellar binary were fitted simultaneously to theoretical isochrones. The uncertainty in M_* quoted by Bakos et al. (2007) is 8%, corresponding to a systematic error of 2.7% in our determinations of R_* and R_p. The planetary mass M_p hardly affects the photometric model at all, since $M_p \ll M_*$, but for completeness we use the previously determined value $M_p = 0.53\,M_{\text{Jup}}$.

To calculate the relative flux as a function of the projected separation of the planet and the star, we employed the analytic formulae of Mandel & Agol (2002) to compute the integral of the

---

[11] Specifically, we used the tables for ATLAS models, interpolating for $T_{\text{eff}} = 5975$ K, $\log g = 4.45$ cgs, $\log[\text{M/H}] = 0.1$, and $v_t = 2.0$ km s^{-1}. For the z band, $a = 0.18$ and $b = 0.34$. We also used these values for the Z band, finding that they provided a good fit. For the I band, $a = 0.22$ and $b = 0.34$.

TABLE 2
System Parameters of HAT-P-1b

Parameter	Value
$(R_*/R_\odot)/(M_*/1.12\ M_\odot)^{1/3}$	1.115 ± 0.034
$(R_p/R_{\rm Jup})/(M_*/1.12\ M_\odot)^{1/3}$	1.203 ± 0.043
i (deg)..	86.22 ± 0.24
M_* ($M_\odot$)	1.12 ± 0.09
M_p ($M_{\rm Jup}$)	0.53 ± 0.04
Velocity semiamplitude K_* (m s^{-1})........	60.3 ± 2.1
Orbital period P (days)...........................	4.46529 ± 0.00009
R_* ($R_\odot$)	1.115 ± 0.043
R_p ($R_{\rm Jup}$)	1.203 ± 0.051
R_p/R_*	0.11094 ± 0.00082
Semimajor axis a (AU)...........................	0.0551 ± 0.0015
$b \equiv a \cos i/R_*$	0.701 ± 0.023
a/R_*	10.64 ± 0.32
a/R_p	95.9 ± 3.5
$t_{\rm IV} - t_{\rm I}$ (hr)...	2.779 ± 0.032
$t_{\rm II} - t_{\rm I}$ (hr)...	0.508 ± 0.035
ρ_* (g cm^{-3})...	1.14 ± 0.10
ρ_p (g cm^{-3})...	0.376 ± 0.031
GM_p/R_p^2 (cm s^{-2})...................................	904.5 ± 66.1

Notes.—This table has three sections. The first three rows list the parameters that were estimated by fitting the new photometric data, as explained in § 3. The orbital eccentricity was assumed to be exactly zero. The next four rows list some parameters from Bakos et al. (2007), reproduced here for convenience. The remainder of the table lists some interesting parameters that can be derived from the parameters in the first two sections.

We did this as follows. The most relevant timescale is ~20 minutes, the ingress or egress duration. First, we calculated σ_1, the standard deviation of the unbinned out-of-transit data. (The results for each light curve are given in Figs. 1 and 2.) Next, we averaged the out-of-transit data into 20 minute bins, with each bin consisting of N data points, depending on the cadence. Then we calculated the standard deviation, σ_N. In the absence of red noise, we would observe $\sigma_N = \sigma_1/\sqrt{N}$, but in practice σ_N is larger than $\sigma_1/\sqrt{N}$ by some factor β. Therefore, we set the data weights equal to $\beta\,\sigma_1$. The exact choice of averaging time did not matter much. In the end, we used the mean value of β over averaging times ranging from 15 to 25 minutes. Typically, we found $\beta \approx 2$, depending on the telescope and sky conditions.[12]

In all cases, to solve for the a posteriori probability distributions of the model parameters, we used a Markov chain Monte Carlo algorithm (see, e.g., Tegmark et al. [2004] for applications to cosmological data, Ford [2005] for radial velocity data, and Holman et al. [2006] or Burke et al. [2007] for a similar approach to transit fitting). We ensured that the Gelman & Rubin (1992) R-statistic was within 0.5% of unity, a sign of good mixing and convergence. For each parameter, we took the median value of the distribution to be our best estimate and the standard deviation as the 1 σ uncertainty.

4. RESULTS

The results are given in Tables 2 and 3. The first of these tables gives the planetary, stellar, and orbital parameters, with the fundamental parameters $R_*/M_*^{1/3}$, $R_p/M_*^{1/3}$, and i listed first. For the parameters that depend on the choice of M_* (namely, R_*, R_p, a, and

TABLE 3
Midtransit Times of HAT-P-1

Observatory	Epoch E	Midtransit time (HJD)	Uncertainty (days)
Lick	-4	2,453,979.92848	0.00069
Lick	-2	2,453,988.86197	0.00076
FLWO.............	0	2,453,997.79200	0.00054
Lick	0	2,453,997.79348	0.00047
FLWO.............	2	2,454,006.72326	0.00059
FLWO.............	3	2,454,011.18837	0.00107
Wise	16	2,454,069.23795	0.00290

Notes.—Based on these new measurements, we derived a transit ephemeris $T_c(E) = T_c(0) + EP$, with $T_c(0) = 2,453,997.79258(29)$ (HJD) and $P = 4.46543(14)$ days, where the numbers in parentheses indicate the 1 σ uncertainty in the final two digits. We note that Bakos et al. (2007) derived a more precise period based on observations over 217 cycles, $P = 4.465290(90)$ days.

ρ_p), we have accounted for the systematic error due to the 8% uncertainty in M_*. Table 3 gives the measured transit times.

4.1. Planetary, Stellar, and Orbital Parameters

We find the stellar radius to be $R_* = 1.115 \pm 0.043\ R_\odot$ and the planetary radius to be $R_p = 1.203 R_{\rm Jup} \pm 0.051 R_{\rm Jup}$. The statistical error is comparable to the systematic error resulting from the covariance with the stellar mass, implying that there is still some scope for improvement through additional high-precision photometry. Our value for the stellar radius agrees well with the value $R_* = 1.15^{+0.10}_{-0.07}\ R_\odot$ determined by Bakos et al. (2007). Those authors estimated R_* from an analysis of the stellar spectrum—its effective temperature, surface gravity, and metallicity—whereas we estimated R_* (actually $R_*/M_*^{1/3}$) by fitting the transit light curves. The agreement between these different methods of determining the stellar radius is an important consistency check on both analyses. Our value for the planetary radius is 1.5 σ' smaller than the previously determined value $R_p = 1.36^{+0.11}_{-0.09} R_{\rm Jup}$, where σ' is the quadrature sum of the statistical errors of the two estimates. Thus, we have revised the planetary radius downward, and we have improved the measurement precision by a factor of 2.

We performed a number of additional optimizations to check the sensitivity of the results to the choice of limb-darkening function. We tried replacing the quadratic law with either a linear law or the four-parameter "nonlinear" law of Claret (2000). For the quadratic law, we tried replacing the ATLAS-based coefficients with the PHOENIX-based coefficients of Claret (2004). In none of these cases did the optimized value of R_p change by more than 0.5% relative to the value presented in Table 2. For the case of the linear law, we tried fitting for the limb-darkening coefficient rather than fixing it at the prescribed value. In that case, R_p increased by 1.8%, which is still small in comparison to the quoted error. (We found that the present data are unable to meaningfully constrain more than one limb-darkening parameter.) We conclude that the systematic error due to the choice of limb-darkening law is probably ~1%.

Also given for convenience in Table 2 are some results reproduced from Bakos et al. (2007), as well as some useful derived quantities. Among these quantities are the impact parameter b, defined as $a \cos i/R_*$ (where a is the semimajor axis), the radius ratio R_p/R_*, the fractions a/R_* and a/R_p, and the stellar mean density ρ_*, which (as mentioned above) do not depend on our choice for M_*. We used the previous measurement of the velocity semiamplitude of the spectroscopic orbit, $K_* = 60.3 \pm 2.1$ m s^{-1}, to calculate the planetary surface gravity, which is also independent

---

[12] This procedure effectively increases the error bar of each measurement and results in a minimum value of $\chi^2/N_{\rm dof}$ that is smaller than unity. It is equivalent to setting σ_j at the value that produces $\chi^2/N_{\rm dof} = 1$ but then using $\Delta\chi^2 = \beta^2$ instead of $\Delta\chi^2 = 1$ to define the 68% confidence limit.
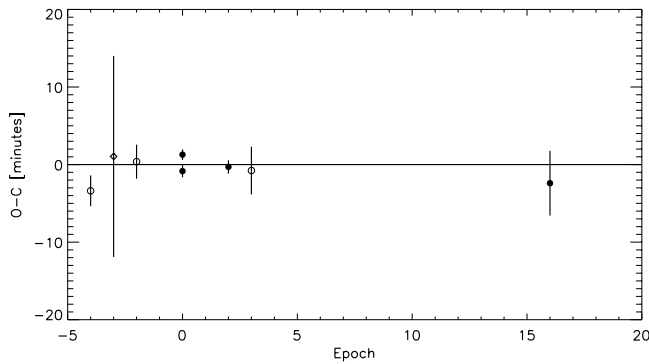
FIG. 3.—Transit timing residuals for HAT-P-1b. The calculated times, using the ephemeris derived in § 4.2, have been subtracted from the observed times. The filled circles represent observations of complete transits. The open circles represent observations of partial transits. The diamond represents the previous observation by Bakos et al. (2007), which was not used in the fit but agrees well with the computed ephemeris.

of the undetermined stellar properties (see, e.g., Southworth et al. 2007; Winn et al. 2007a). The results for a and the planetary mean density ρ_p do depend on the choice of stellar mass, and in those cases the quoted errors have been enlarged appropriately to take this extra source of uncertainty into account. For convenience in planning future observations, we give the calculated values of the full transit duration (the time between first and fourth contact, $t_{IV} - t_I$) and the partial transit duration (the time between first and second contact or between third and fourth contact).[13]

4.2. Transit Times

Table 3 gives the transit times measured from our data. We used these times to calculate a photometric ephemeris for this system. Using only our seven new measurements, we fitted a linear function of transit epoch E,

$$T_c(E) = T_c(0) + EP. \qquad (4)$$

The fit had $\chi^2/N_{dof} = 1.6$ and $N_{dof} = 5$, suggesting that either the period is not exactly constant or the transit time uncertainties have been underestimated. Because one would prefer to have an ephemeris with conservative error estimates for planning future observations, we rescaled the measurement errors by $(1.6)^{1/2}$ and refitted the ephemeris, finding $T_c(0) = 2,453,997.79258(29)$ (HJD) and $P = 4.46543(14)$ days. The numbers in parentheses indicate the 1 σ uncertainty in the final two digits. Our derived period agrees with the value 4.465290(90) days determined by Bakos et al. (2007), within the respective 1 σ limits. Figure 3 is the $O - C$ (observed minus calculated) diagram for the transit times.

5. SUMMARY AND DISCUSSION

We have presented new photometry of HAT-P-1 spanning the times of transit of its close-in giant planet. The photometry improves the precision with which the stellar and planetary radii are known by a factor of 2 and places the measurements on a more robust footing by determining the stellar mean density directly from the photometric data. We have also updated the transit ephemeris to help in planning future observations.

---

[13] Although the partial transit duration is listed as $t_{II} - t_I$ in Table 1, all of the results in Table 1 are based on the entire light curves, including both ingress and egress data. Our model assumes $t_{II} - t_I = t_{IV} - t_{III}$.

Although the revised planetary radius is somewhat lower than the previously determined value, the planet HAT-P-1b is still among the largest and least dense of the known transiting exoplanets. Its mean density (0.376 ± 0.031 g cm^{-3}) is comparable to that of the famously oversized planet HD 209458b (0.35 g cm^{-3}; Knutson et al. 2007a). A third planet with a comparably low mean density is WASP-1b (0.36 g cm^{-3}; Collier Cameron et al. 2007; Charbonneau et al. 2007; Shporer et al. 2007).

There is an extensive literature on the interpretation of exoplanetary radii, in particular on the subject of these apparently "bloated" planets. This term refers to the apparent conflict (of order 10%–20%) between the measured planetary radii and the calculated radii using simple structural models for hydrogen/helium planets of the appropriate mass, temperature, age, and degree of external heating by the parent star. Many mechanisms have been proposed to sustain hotter gaseous envelopes and therefore larger planets: the efficient delivery of heat from the star to the planetary interior (Guillot & Showman 2002; Showman & Guillot 2002), the production of internal heat by tidal interactions (Bodenheimer et al. 2003; Winn & Holman 2005), and the trapping of internal heat by enhanced atmospheric opacities (Burrows et al. 2007) or inhibited convection (Chabrier & Baraffe 2007). Only the tidal mechanisms have been specific or predictive enough to be ruled out; the obliquity tide theory of Winn & Holman (2005) did not withstand more detailed dynamical analysis (Levrard et al. 2007; Fabrycky et al. 2007), and the eccentricity tide mechanism of Bodenheimer et al. (2003) does not seem to be operative in the case for which it was invented, HD 209458b (Laughlin et al. 2005). Which (if any) of the other mechanisms contribute to the observed radii of transiting exoplanets is not yet clear.

However, for HAT-P-1b, this issue may be a red herring. We find that there is no strong conflict with structural models at this point, as long as the planet does not have a massive core of heavy elements. Burrows et al. (2007) recently computed models for many of the transiting exoplanets, in particular HAT-P-1b, taking into account the appropriate planetary mass, orbital distance, stellar luminosity, stellar spectrum, and stellar age. Assuming a planet of solar composition, an atmosphere of standard solar-composition opacity, and no dense heavy-element core, they calculated $R_p = 1.18R_{Jup}$–$1.22R_{Jup}$ over the plausible age range 3.5 ± 1.0 Gyr. This range of calculated values for R_p comfortably overlaps the 1 σ range in our measured value, $1.203R_{Jup} \pm 0.051R_{Jup}$.

Fortney et al. (2007) have also provided theoretical estimates of exoplanetary radii over a wide range of conditions, although they are not specifically tuned for any particular cases of the known exoplanets. For a coreless H/He planet with mass $0.5M_{Jup}$ orbiting a 3 Gyr old solar-luminosity star at a distance of 0.045 AU (and thereby receiving nearly the same flux as HAT-P-1, which orbits an ~ 1.5 $L_\odot$ star at a distance of 0.055 AU), Fortney et al. (2007) predict a planetary radius $R_p = 1.12R_{Jup}$. This is smaller than the value computed by Burrows et al. (2007), and at least part of the reason for the difference is that Fortney et al. (2007) did not account for the "transit radius effect," the enlarged size of the transit-measured radius relative to the $\tau = 2/3$ photosphere that is usually taken to be the "radius" by theoreticians. This effect amounts to a few percent in the planetary radius (see also Burrows et al. 2003). Assuming that this effect adds between 0% and 5% to the calculated radius, the difference between the calculated radius of R_p and our measured value is 0.5–1.6 σ, i.e., not very significant.

We conclude that the present data are consistent with current models of coreless, solar-composition, strongly irradiated giant planets. Bakos et al. (2007) estimated a stellar metallicity of $Z = 0.025$, i.e., comparable to the Sun, and hence the inference of a small or absent core is broadly consistent with the core-metallicity

relation proposed by Guillot et al. (2006). Of course, there are many other possibilities that are also consistent with the data, such as a planet with a dense core that also has either an extra source of atmospheric opacity or an extra source of internal heat. As of now there is no way to distinguish among these possibilities.

As discussed by Burrows et al. (2007), it is becoming clear that there are many determinants of planetary radii. By considering the entire ensemble of exoplanets, one can fully appreciate the strengths and weaknesses of theoretical models and possibly obtain clues about interesting processes that may have been overlooked. This requires not only the discovery of new transiting systems but also high-precision determinations of the system parameters, such as the present study.

REFERENCES

Baines, E. K., van Belle, G. T., ten Brummelaar, T. A., McAlister, H. A., Swain, M., Turner, N. H., Sturmann, L., & Sturmann, J. 2007, ApJ, 661, L195
Bakos, G. Á., et al. 2007, ApJ, 656, 552
Bodenheimer, P., Laughlin, G., & Lin, D. N. C. 2003, ApJ, 592, 555
Burke, C. J., et al. 2007, ApJ, submitted (arXiv: 0705.0003)
Burrows, A., Hubeny, I., Budaj, J., & Hubbard, W. B. 2007, ApJ, 661, 502
Burrows, A., Sudarsky, D., & Hubbard, W. B. 2003, ApJ, 594, 545
Butler, R. P., Marcy, G. W., Williams, E., Hauser, H., & Shirts, P. 1997, ApJ, 474, L115
Butler, R. P., et al. 2006, ApJ, 646, 505
Chabrier, G., & Baraffe, I. 2007, ApJ, 661, L81
Charbonneau, D., Brown, T. M., Burrows, A., & Laughlin, G. 2007, in Protostars and Planets V, ed. B. Reipurth, D. Jewitt, & K. Keil (Tucson: Univ. Arizona Press), 701
Charbonneau, D., Brown, T. M., Latham, D. W., & Mayor, M. 2000, ApJ, 529, L45
Charbonneau, D., Winn, J. N., Everett, M. E., Latham, D. W., Holman, M. J., Esquerdo, G. A., & O'Donovan, F. T. 2007, ApJ, 658, 1322
Claret, A. 2000, A&A, 363, 1081
———. 2004, A&A, 428, 1001
Collier Cameron, A. C., et al. 2007, MNRAS, 375, 951
Fabrycky, D. C., Johnson, E. T., & Goodman, J. 2007, ApJ, 665, 754
Ford, E. B. 2005, AJ, 129, 1706
Fortney, J. J., Marley, M. S., & Barnes, J. W. 2007, ApJ, 659, 1661
Gelman, A., & Rubin, D. B. 1992, Statis. Sci., 7, 457
Gillon, M., Pont, F., Moutou, C., Bouchy, F., Courbin, F., Sohy, S., & Magain, P. 2006, A&A, 459, 249
Grillmair, C. J., Charbonneau, D., Burrows, A., Armus, L., Stauffer, J., Meadows, V., Van Cleve, J., & Levine, D. 2007, ApJ, 658, L115
Guillot, T., Santos, N. C., Pont, F., Iro, N., Melo, C., & Ribas, I. 2006, A&A, 453, L21

Guillot, T., & Showman, A. P. 2002, A&A, 385, 156
Henry, G. W., Marcy, G. W., Butler, R. P., & Vogt, S. S. 2000, ApJ, 529, L41
Holman, M. J., et al. 2006, ApJ, 652, 1715
———. 2007, ApJ, 664, 1185
Knutson, H. A., Charbonneau, D., Noyes, R. W., Brown, T. M., & Gilliland, R. L. 2007a, ApJ, 655, 564
Knutson, H., et al. 2007b, Nature, 447, 183
Laughlin, G., Marcy, G. W., Vogt, S. S., Fischer, D. A., & Butler, R. P. 2005, ApJ, 629, L121
Levrard, B., Correia, A. C. M., Chabrier, G., Baraffe, I., Selsis, F., & Laskar, J. 2007, A&A, 462, L5
Mandel, K., & Agol, E. 2002, ApJ, 580, L171
Mayor, M., & Queloz, D. 1995, Nature, 378, 355
Pinfield, D. J., Hodgkin, S. T., Jameson, R. F., Cossburn, M. R., & von Hippel, T. 1997, MNRAS, 287, 180
Pont, F., et al. 2007, A&A, 465, 1069
Richardson, L. J., Deming, D., Horning, K., Seager, S., & Harrington, J. 2007, Nature, 445, 892
Seager, S., & Mallén-Ornelas, G. 2003, ApJ, 585, 1038
Showman, A. P., & Guillot, T. 2002, A&A, 385, 166
Shporer, A., Tamuz, O., Zucker, S., & Mazeh, T. 2007, MNRAS, 376, 1296
Southworth, J., Wheatley, P. J., & Sams, G. 2007, MNRAS, 379, L11
Sozzetti, A., Torres, G., Charbonneau, D., Latham, D. W., Holman, M. J., Winn, J. N., Laird, J. B., & O'Donovan, F. T. 2007, ApJ, 664, 1190
Tegmark, M., et al. 2004, Phys. Rev. D, 69, 103501
Winn, J. N., & Holman, M. J. 2005, ApJ, 628, L159
Winn, J. N., et al. 2007a, AJ, 133, 1828
———. 2007b, AJ, 133, 11